Coupling Matrix Compression Technique for High-Isolation Dual-mode Dual-band Filters

Pengyu Ma, *Student Member, IEEE,* Bin Wei, *Member, IEEE,* Jiasheng Hong, *Fellow, IEEE,* Xubo Guo, *Member, IEEE,* Bisong Cao, and Linan Jiang

***Abstract*—This paper proposes a new coupling matrix synthesis technique called the coupling matrix compression technique, which focuses on reducing the dimension of the $N+2$ coupling matrix. The presented coupling matrices can be compressed, and this technique can be used to design dual-mode resonators for high-isolation dual-band filters. One dual-mode resonator is represented as two closely coupled resonators when using this technique. The formulae for resonant frequencies and ω_m in dual-mode theory are also derived in this paper. A dual-mode embedded hairpin resonator is designed and analyzed using this technique, and a dual-band filter using the proposed resonators is designed and fabricated to validate the proposed technique.**

***Index Terms*—Coupling matrix for filter synthesis, dimension, dual-mode, dual-band, microwave filters.**

I. Introduction

THE coupling matrix theory is a powerful mathematical tool in modern microwave filters design. Many researchers are interested in this field of study [1]–[6] and typically use matrix rotation and optimization [7] during coupling matrix transformations. However, these synthesis methods are confined to use with matrix transformations of matrices with dimensions of $n+2$ to $n+2$. Thus, these methods are inconvenient to reduce the dimension of large-order matrices.

Some papers use coupling matrix synthesis to design dual-band filters [8]–[10]. A single-band can be split into two bands using transmission zeros, which can be produced by cross couplings. To obtain a feasible coupling topology, synthesis is used to optimize and reconfigure the coupling structure. However, conventional methods cannot eliminate cross-couplings, and a special topology is still needed when using these methods. Thus, it is difficult to implement a synthesized topology, especially with planar microstrip technology.

In this paper, a new coupling matrix synthesis method is presented to reduce the dimension of the coupling matrix. And it would not change the S-parameter responses of the matrix. When two single-mode resonators are closely coupled, they can be considered to be a dual-mode resonator, which reduces the number of resonators and effectively compresses the coupling matrix. Following dual-mode cascading theory [11], this paper focuses on the characteristics of dual-mode resonators. Using the coupling matrix compression technique, dual-mode resonators can be analyzed theoretically. The formulae of the resonant frequencies and ω_m in dual-mode theory are derived in this paper.

Notably, not all the coupling matrices can be compressed. This paper finds that the matrices with special topologies can be compressed, such as peninsula topology, discussed in Section II-B and proportional topology, discussed in Section II-C. Using the topology proposed in this paper, the ω_m in the dual-mode theory is shown to be between the two resonant frequencies, indicating that these dual-mode resonators can be used for high-isolation dual-mode dual-band filters.

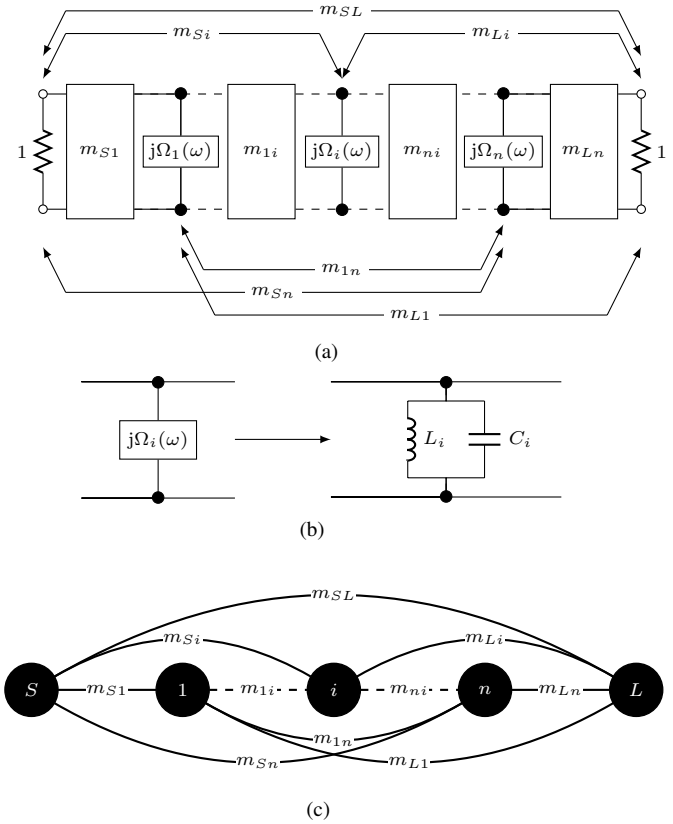

Fig. 1. (a) Circuit model for the n-node filter. (b) $\Omega_i(\omega)$ is replaced by an LC circuit. (c) Topology model for the n-resonators filter.

Manuscript received XXX, 2016. This work was supported by the National Natural Science Foundation of China under Grant 61371009 and the National Key Scientific Instrument and Equipment Development Project of China (Grant No.2014YQ030975)

P. Ma, B. Wei, X. Guo, B. Cao, and L. Jiang are with the State Key Laboratory of Low-Dimensional Quantum Physics, Department of Physics, Tsinghua University, Beijing 100084, China (e-mail: mapy15@mails.tsinghua.edu.cn; weibin@mail.tsinghua.edu.cn)

J. Hong is with the Institute of Signal, Sensors, and Systems (ISSS), School of Engineering and Physical Sciences, Heriot-Watt University, Edinburgh EH14 4AS, U.K. (e-mail: j.hong@hw.ac.uk).

II. Matrix Compression Technique

This section discusses a few matrix transformation techniques and derives the matrix compression technique. To simplify the derivation process, all impedances or admittances in the circuit models are normalized by input/output impedances.

A. Basic Coupling Matrix Theory

Considering a fully coupled filter with n resonators, the general circuit model is shown in Fig. 1(a), where m_{ij} is the admittance inverter between node i and j; and $\mathrm{j}\Omega_i(\omega)$ is the admittance in node i. For a single-mode resonator, $\mathrm{j}\Omega_i(\omega)$ is typically replaced by an LC circuit, shown in Fig. 1(b). Then,

$$\mathrm{j}\Omega_i(\omega) = \mathrm{j}C_i\omega + \frac{1}{\mathrm{j}L_i\omega} = \mathrm{j}\sqrt{\frac{C_i}{L_i}}\frac{\omega^2 - \frac{1}{L_iC_i}}{\omega\sqrt{\frac{1}{L_iC_i}}} = \mathrm{j}\gamma_i\frac{\omega^2-\omega_i^2}{\omega_i\omega} \tag{1}$$

where $\gamma_i = \sqrt{C_i/L_i}$ and $\omega_i = \sqrt{1/L_iC_i}$.

The conventional way to form a single-band response is making

$$\omega_i = \omega_0, \quad \gamma_i = \frac{1}{FBW} \tag{2}$$

for $i = 1, 2, 3, \ldots, n$, where ω_0 is the central frequency of this pass-band and FBW is the fractional bandwidth.

Fig. 1(c) shows the topology of the circuit in Fig. 1(a). The $[A]$-matrix defined in [12, p.229] is shown in (3). The rows and columns of the $[A]$-matrix start counting from zero.

$$A = \begin{array}{c} \begin{matrix} 0(S) & 1 & \cdots & i & \cdots & n+1(L) \end{matrix} \\ \begin{bmatrix} -\mathrm{j} & m_{S1} & \cdots & m_{Si} & \cdots & m_{SL} \\ m_{S1} & \Omega_1(\omega) & \cdots & m_{1i} & \cdots & m_{L1} \\ \vdots & \vdots & \ddots & \vdots & \ddots & \vdots \\ m_{Si} & m_{1i} & \cdots & \Omega_i(\omega) & \cdots & m_{Li} \\ \vdots & \vdots & \ddots & \vdots & \ddots & \vdots \\ m_{Sn} & m_{1n} & \cdots & m_{ni} & \cdots(\omega) & m_{Ln} \\ m_{SL} & m_{L1} & \cdots & m_{Li} & \cdots & -\mathrm{j} \end{bmatrix} \end{array} \begin{matrix} S \\ 1 \\ \vdots \\ i \\ \vdots \\ n \\ L \end{matrix} \tag{3}$$

Then, from [12, p.229], the following can be derived:

$$\begin{aligned} S_{21}(A) &= -2\mathrm{j}[A]^{-1}_{n+1,0} \\ S_{11}(A) &= 1 + 2\mathrm{j}[A]^{-1}_{0,0} \end{aligned} \tag{4}$$

Different $[A]$-matrices may lead to the same response. If $[A']$ has the same response with $[A]$, which means

$$\begin{aligned} S_{21}(A') &= S_{21}(A), \quad S_{12}(A') = S_{12}(A) \\ S_{11}(A') &= S_{11}(A), \quad S_{22}(A') = S_{22}(A) \end{aligned} \tag{5}$$

$[A']$ and $[A]$ are equivalent, described by:

$$[A] \equiv [A'] \tag{6}$$

Equivalent transforms are useful to create an equivalent $[A]$-matrix.

One equivalent transform is the similarity transform proposed in [3]:

$$[A'] = [R^\theta_{i,j}][A][R^\theta_{i,j}]^{\mathrm{T}} \tag{7}$$

where $[R^\theta_{i,j}]$ is the rotation matrix, defined in (8), and $[R^\theta_{i,j}]^{\mathrm{T}}$ is its transpose. It has a pivot, $[i,j]$ ($i \neq j,\ i,j \neq 0$ and $n+1$) and an angle of rotation, θ.

$$R^\theta_{i,j} = \begin{array}{c} \begin{matrix} 1 & 0 & \cdots & 0 & \cdots & 0 & \cdots & 0 \end{matrix} \\ \begin{bmatrix} 1 & 0 & \cdots & 0 & \cdots & 0 & \cdots & 0 \\ 0 & 1 & \cdots & 0 & \cdots & 0 & \cdots & 0 \\ \vdots & \vdots & \ddots & \vdots & \ddots & \vdots & \ddots & \vdots \\ 0 & 0 & \cdots & \cos(\theta) & \cdots & -\sin(\theta) & \cdots & 0 \\ \vdots & \vdots & \ddots & \vdots & \ddots & \vdots & \ddots & \vdots \\ 0 & 0 & \cdots & \sin(\theta) & \cdots & \cos(\theta) & \cdots & 0 \\ \vdots & \vdots & \ddots & \vdots & \ddots & \vdots & \ddots & \vdots \\ 0 & 0 & \cdots & 0 & \cdots & 0 & \cdots & 1 \end{bmatrix} \end{array} \begin{matrix} S \\ 1 \\ \vdots \\ i \\ \vdots \\ j \\ \vdots \\ L \end{matrix} \\ \begin{matrix} S & 1 & \cdots & i & \cdots & j & \cdots & L \end{matrix} \tag{8}$$

After rotation, the elements in rows i and j, and columns i and j of $[A]$ are changed. The values in $[A']$ are changed as follows:

$$\begin{aligned} A'_{ki} =& A'_{ik} = \cos(\theta)A_{ik} - \sin(\theta)A_{jk} \\ A'_{kj} =& A'_{jk} = \sin(\theta)A_{ik} + \cos(\theta)A_{jk} \\ A'_{ii} =& \cos^2(\theta)A_{ii} - 2\sin(\theta)\cos(\theta)A_{ij} + \sin^2(\theta)A_{jj} \\ A'_{jj} =& \sin^2(\theta)A_{ii} + 2\sin(\theta)\cos(\theta)A_{ij} + \cos^2(\theta)A_{jj} \\ A'_{ij} =& (\cos^2(\theta) - \sin^2(\theta))A_{ij} + \sin(\theta)\cos(\theta)(A_{ii} - A_{jj}) \\ A'_{ji} =& A'_{ij} \end{aligned} \tag{9}$$

where $k(\neq i,j) = 0, 1, \ldots, n+1$.

This paper proposes another equivalent transform called the scaling transform, which is defined as follows:

$$[A'] = [S^\alpha_i][A][S^\alpha_i]^{\mathrm{T}} \tag{10}$$

where $[S^\alpha_i]$ is the scaling matrix defined in (11), and $[S^\alpha_i]^{\mathrm{T}}$ is its transpose. It is a diagonal matrix with all diagonal entries equal to 1, except for the entry at $[i,i]$, ($i \neq 0$ and $n+1$):

$$S^\alpha_i = \begin{array}{c} \begin{matrix} S & 1 & \cdots & i & \cdots & n & L \end{matrix} \\ \begin{bmatrix} 1 & & & & & & \\ & 1 & & & & \mathbf{0} & \\ & & \ddots & & & & \\ & & & \alpha & & & \\ & & & & \ddots & & \\ & \mathbf{0} & & & & 1 & \\ & & & & & & 1 \end{bmatrix} \end{array} \begin{matrix} S \\ 1 \\ \vdots \\ i \\ \vdots \\ n \\ L \end{matrix} \tag{11}$$

After this transform, the elements in row i and column i of $[A]$ are changed. The values in $[A']$ are changed as follows:

$$\begin{aligned} A'_{ki} =& A'_{ik} = \alpha A_{ik} \\ A'_{ii} =& \alpha^2 A_{ii} \end{aligned} \tag{12}$$

where $k(\neq i) = 0, 1, \ldots, n+1$.

The proof of this transform is shown in Appendix A.

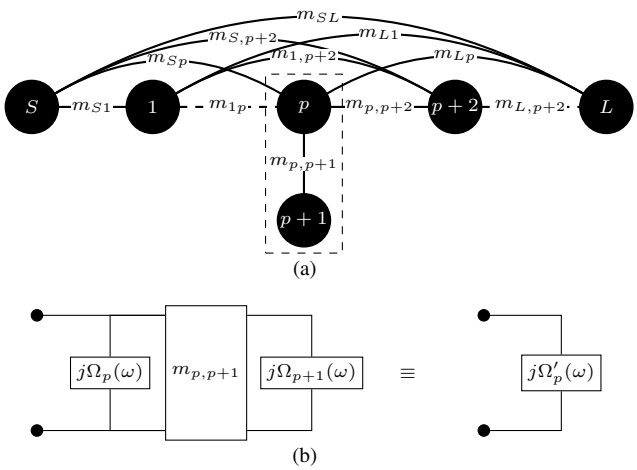

Fig. 2. (a) Peninsula topology. (b) The circuit in the dashed frame and its equivalent circuit.

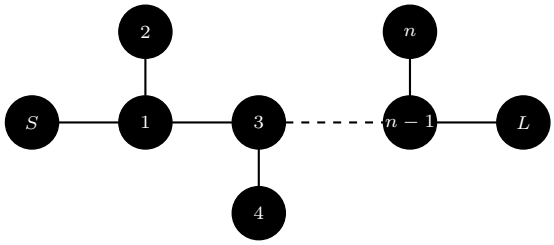

Fig. 3. Topology composed of peninsulas.

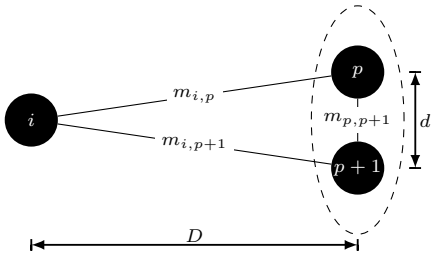

Fig. 4. The proportional topology.

B. Compression Theory for Peninsula Topology

As shown in Fig. 2(a), the peninsula topology is compressible. The resonators, p and $p+1$, form a peninsula, which means that:

$$m_{p+1,k} = 0 \tag{13}$$

for $k(\neq p, p+1) = 0, 1, \ldots, n+1$.

The $[A]$-matrix of this topology can be written as:

$$A = \begin{bmatrix} -\mathrm{j} & m_{S1} & \cdots & m_{Sp} & 0 & \cdots & m_{SL} \\ m_{S1} & \Omega_1 & \cdots & m_{1p} & 0 & \cdots & m_{L1} \\ \vdots & \vdots & \ddots & \vdots & \vdots & \ddots & \vdots \\ m_{Sp} & m_{1p} & \cdots & \Omega_p & m_{p,p+1} & \cdots & m_{Lp} \\ 0 & 0 & \cdots & m_{p,p+1} & \Omega_{p+1} & \cdots & 0 \\ \vdots & \vdots & \ddots & \vdots & \vdots & \ddots & \vdots \\ m_{SL} & m_{L1} & \cdots & m_{Lp} & 0 & \cdots & -\mathrm{j} \end{bmatrix} \tag{14}$$

The circuit of this peninsula shown in Fig. 2(b) is used to compress this $[A]$-matrix. From [13], this peninsula circuit can be replaced by a new frequency variable, Ω'_p, which can be expressed as follows:

$$\Omega'_p = \Omega_p - \frac{m^2_{p,p+1}}{\Omega_{p+1}} \tag{15}$$

After replacement, the number of nodes has been reduced in the topology. The $(n+2)\times(n+2)$ $[A]$-matrix has also transformed into $(n+1)\times(n+1)$ $[A']$:

$$A' = \begin{bmatrix} -\mathrm{j} & m_{S1} & \cdots & m_{Sp} & \cdots & m_{SL} \\ m_{S1} & \Omega_1 & \cdots & m_{1p} & \cdots & m_{L1} \\ \vdots & \vdots & \ddots & \vdots & \ddots & \vdots \\ m_{Sp} & m_{1p} & \cdots & \Omega'_p & \cdots & m_{Lp} \\ \vdots & \vdots & \ddots & \vdots & \ddots & \vdots \\ m_{SL} & m_{L1} & \cdots & m_{Lp} & \cdots & -\mathrm{j} \end{bmatrix} \tag{16}$$

Then, the rows p and $p+1$ are compressed into one row, and the columns p and $p+1$ are compressed into one column. This replacement does not change the response, so

$$[A] \equiv [A'] \tag{17}$$

A useful dual-band topology composed by the peninsulas is shown in Fig. 3. In this topology, we can iterate the above steps and compress the $[A]$-matrix from $(n+2)\times(n+2)$ finally into dimension $(n/2+2)\times(n/2+2)$. Some examples using this topology to design dual-band resonators are shown in [13]–[15].

C. Compression Theory for Proportional Topology

A more general condition can be described by:

$$m_{p+1,k} = \lambda m_{p,k} \tag{18}$$

for $k(\neq p, p+1) = 0, 1, \ldots, n+1$.

Equation (13) is a special case of (18) when $\lambda = 0$.

Two closely coupled single resonators can be considered to be one dual-mode resonator, as shown in Fig. 4. This type of dual-mode resonator matches the above mentioned proportional condition. In Fig. 4, resonator i is an arbitrary resonator in the filter, p and $p+1$ are the closely coupled resonators when $d << D$. The coupling coefficient for two resonators is determined by the distance and current distribution at the resonant frequencies. They can be roughly described in the following form, when the distance, D, is sufficiently large [16]–[19].

$$\begin{aligned} m_{i,p} &= C_{i,p} D_{i,p}^{-\alpha} \approx C_{i,p} D^{-\alpha} \\ m_{i,p+1} &= C_{i,p+1} D_{i,p+1}^{-\alpha} \approx C_{i,p+1} D^{-\alpha} \end{aligned} \tag{19}$$

where $C_{i,p}$, $C_{i,p+1}$ and α are the coefficients determined by the current distribution of the coupled resonators, and for parallel-coupled line, $\alpha = 1$; $D_{i,p}$ is the distance between the resonator i and p, and $D_{i,p+1}$ is the distance between the resonator i and $p+1$.

So,

$$\lambda = \frac{m_{i,p+1}}{m_{i,p}} = \frac{C_{i,p+1}}{C_{i,p}} \tag{20}$$

Then, the λ is not affected by the distance. And if we use similar resonators, λ does not change with i.

To compress this type of topology, the $[A]$-matrix can be rewritten as $[A^0]$:

$$A^0 = \begin{bmatrix} -\mathrm{j} & m_{S1} & \cdots & m_{Sp} & \lambda m_{Sp} & \cdots & m_{SL} \\ m_{S1} & \Omega_1 & \cdots & m_{1p} & \lambda m_{1p} & \cdots & m_{L1} \\ \vdots & \vdots & \ddots & \vdots & \vdots & \ddots & \vdots \\ m_{Sp} & m_{1p} & \cdots & \Omega_p & m_{p,p+1} & \cdots & m_{Lp} \\ \lambda m_{Sp} & \lambda m_{1p} & \cdots & m_{p,p+1} & \Omega_{p+1} & \cdots & \lambda m_{Lp} \\ \vdots & \vdots & \ddots & \vdots & \vdots & \ddots & \vdots \\ m_{SL} & m_{L1} & \cdots & m_{Lp} & \lambda m_{Lp} & \cdots & -\mathrm{j} \end{bmatrix} \tag{21}$$

Then, a similarity transform, $[R^{\theta_0}_{p,p+1}]$ is performed on $[A^0]$, where $\theta_0 = -\arctan(\lambda)$. From (7):

$$[A^1] = [R^{\theta_0}_{p,p+1}][A^0][R^{\theta_0}_{p,p+1}]^{\mathrm{T}} \tag{22}$$

From (9), the following can be derived:

$$\begin{aligned} A^1_{kp} &= A^1_{pk} = \frac{m_{pk}}{\cos(\theta_0)} \\ A^1_{k,p+1} &= A^1_{p+1,k} = 0 \\ A^1_{p,p} &= \frac{\Omega_p + 2\lambda m_{p,p+1} + \lambda^2 \Omega_{p+1}}{1+\lambda^2} \\ A^1_{p+1,p+1} &= \frac{\lambda^2 \Omega_p - 2\lambda m_{p,p+1} + \Omega_{p+1}}{1+\lambda^2} \\ A^1_{p,p+1} &= A^1_{p+1,p} = \frac{1-\lambda^2}{1+\lambda^2} m_{p,p+1} - \frac{\lambda}{1+\lambda^2}(\Omega_p - \Omega_{p+1}) \end{aligned} \tag{23}$$

for $k(\neq p, p+1) = 0, 1, \ldots, n+1$.

Thus,

$$A^1 = \begin{bmatrix} -\mathrm{j} & m_{S1} & \cdots & \frac{m_{Sp}}{\cos(\theta_0)} & 0 & \cdots & m_{SL} \\ m_{S1} & \Omega_1 & \cdots & \frac{m_{1p}}{\cos(\theta_0)} & 0 & \cdots & m_{L1} \\ \vdots & \vdots & \ddots & \vdots & \vdots & \ddots & \vdots \\ \frac{m_{Sp}}{\cos(\theta_0)} & \frac{m_{1p}}{\cos(\theta_0)} & \cdots & \Omega'_p & M & \cdots & \frac{m_{Lp}}{\cos(\theta_0)} \\ 0 & 0 & \cdots & M & \Omega'_{p+1} & \cdots & 0 \\ \vdots & \vdots & \ddots & \vdots & \vdots & \ddots & \vdots \\ m_{SL} & m_{L1} & \cdots & \frac{m_{Lp}}{\cos(\theta_0)} & 0 & \cdots & -\mathrm{j} \end{bmatrix} \tag{24}$$

where

$$\Omega'_p = A^1_{p,p}, \quad \Omega'_{p+1} = A^1_{p+1,p+1}, \quad M = A^1_{p,p+1} \tag{25}$$

Then, scaling transform, $S_p^{\cos(\theta_0)}$ is performed on $[A^1]$. From (10):

$$[A^2] = [S_p^{\cos(\theta_0)}][A^1][S_p^{\cos(\theta_0)}]^{\mathrm{T}} \tag{26}$$

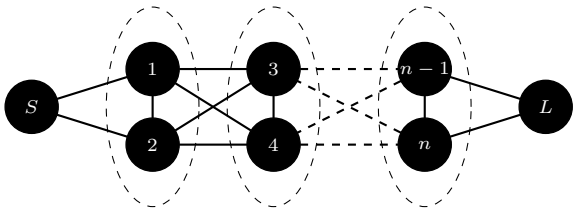

Fig. 5. Topology composed of dual-mode resonators.

From (12),

$$\begin{aligned} A^2_{k,p} &= A^2_{p,k} = m_{p,k} \\ A^2_{p,p} &= \cos^2(\theta_0)\Omega'_p \\ A^2_{p+1,p} &= A^2_{p,p+1} = M\cos(\theta_0) \end{aligned} \tag{27}$$

for $k(\neq p, p+1) = 0, 1, \ldots, n+1$.

Thus,

$$A^2 = \begin{bmatrix} -\mathrm{j} & m_{S1} & \cdots & m_{Sp} & 0 & \cdots & m_{SL} \\ m_{S1} & \Omega_1 & \cdots & m_{1p} & 0 & \cdots & m_{L1} \\ \vdots & \vdots & \ddots & \vdots & \vdots & \ddots & \vdots \\ m_{Sp} & m_{1p} & \cdots & \cos^2(\theta_0)\Omega'_p & \cos(\theta_0)M & \cdots & m_{Lp} \\ 0 & 0 & \cdots & \cos(\theta_0)M & \Omega'_{p+1} & \cdots & 0 \\ \vdots & \vdots & \ddots & \vdots & \vdots & \ddots & \vdots \\ m_{SL} & m_{L1} & \cdots & m_{Lp} & 0 & \cdots & -\mathrm{j} \end{bmatrix} \tag{28}$$

Notably, the $[A^2]$ contains a peninsula. Using (17), the $(n+2)\times(n+2)$ matrix can thus be compressed into a $(n+1)\times(n+1)$ matrix as follows:

$$A^3 = \begin{bmatrix} -\mathrm{j} & m_{S1} & \cdots & m_{Sp} & \cdots & m_{SL} \\ m_{S1} & \Omega_1 & \cdots & m_{1p} & \cdots & m_{L1} \\ \vdots & \vdots & \ddots & \vdots & \ddots & \vdots \\ m_{Sp} & m_{1p} & \cdots & \Omega''_p & \cdots & m_{Lp} \\ \vdots & \vdots & \ddots & \vdots & \ddots & \vdots \\ m_{SL} & m_{L1} & \cdots & m_{Lp} & \cdots & -\mathrm{j} \end{bmatrix} \tag{29}$$

where

$$\begin{aligned} \Omega''_p &= \cos^2(\theta_0)(\Omega'_p - \frac{M^2}{\Omega'_{p+1}}) \\ &= \frac{\Omega_p \Omega_{p+1} - m^2_{p,p+1}}{\lambda^2 \Omega_p + \Omega_{p+1} - 2\lambda m_{p,p+1}} \end{aligned} \tag{30}$$

Another useful dual-band topology composed of dual-mode resonators is shown in Fig. 5. By iterating through the above steps, the $[A]$-matrix is compressed from $(n+2)\times(n+2)$ to $(n/2+2)\times(n/2+2)$. Then, if the two single-mode resonators have resonant frequencies at ω_a and ω_b, their transformed frequencies can be described by the following using a narrow-range approximation:

$$\begin{aligned} \Omega_a(\omega) &= \gamma_a \frac{\omega^2 - \omega_a^2}{\omega_a \omega} \approx \gamma_a \frac{\omega^2 - \omega_a^2}{\omega^2} \\ \Omega_b(\omega) &= \gamma_b \frac{\omega^2 - \omega_b^2}{\omega_b \omega} \approx \gamma_b \frac{\omega^2 - \omega_b^2}{\omega^2} \end{aligned} \tag{31}$$

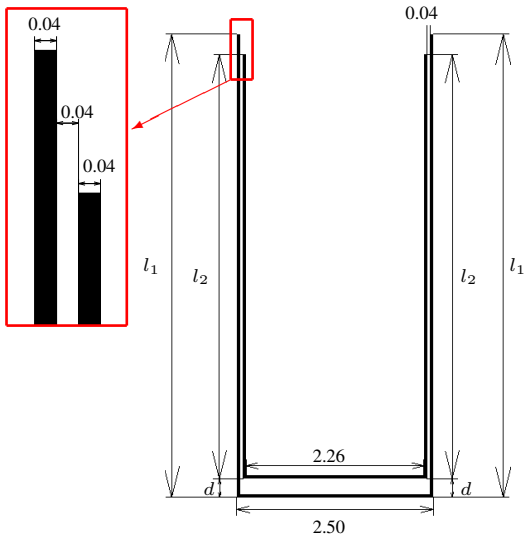

Fig. 6. Layout of the embedded hairpin resonator. (dimensions in mm, line width=0.04 mm).

When these two resonators are coupled and considered to be a dual-mode resonator, the transformed frequencies can be represented by the following using (30),

$$\begin{aligned}\Omega_{dual} &= \frac{\Omega_a\Omega_b - m^2}{\lambda^2\Omega_a + \Omega_b - 2\lambda m} \\ &= \frac{\gamma_a\gamma_b(\omega^2-\omega_a^2)(\omega^2-\omega_b^2) - m^2\omega^4}{\omega^2(\lambda^2\gamma_a(\omega^2-\omega_a^2)+\gamma_b(\omega^2-\omega_b^2) - 2\lambda m\omega^2)} \\ &= \gamma\frac{(\omega^2-\omega_1^2)(\omega^2-\omega_2^2)}{\omega^2(\omega^2-\omega_m^2)}\end{aligned} \tag{32}$$

where m is the coupling coefficient between the two resonators; and:

$$\begin{aligned}\gamma &= \frac{\gamma_a\gamma_b - m^2}{\gamma_a\lambda^2 + \gamma_b - 2\lambda m} \\ \omega_m^2 &= \frac{\gamma_a\lambda^2\omega_a^2 + \gamma_b\omega_b^2}{\gamma_a\lambda^2 + \gamma_b - 2\lambda m} \\ \omega_1^2 + \omega_2^2 &= \gamma_a\gamma_b\frac{\omega_a^2+\omega_b^2}{\gamma_a\gamma_b - m^2} \\ \omega_1^2\omega_2^2 &= \frac{\gamma_a\gamma_b\omega_a^2\omega_b^2}{\gamma_a\gamma_b - m^2}\end{aligned} \tag{33}$$

Equation (32) is the same as that shown in [11]. For most cases, $\gamma_a, \gamma_b > 0$. Appendix B proves that dual-mode resonators, which exhibit the topology shown in Fig. 5 have an ω_m between ω_1 and ω_2 ,when $\gamma_a, \gamma_b > 0$, which can produce high-isolation between these two bands.

III. A Dual-mode Dual-band Example

Two single-mode hairpin resonators are closely coupled to form a dual-mode resonator, as shown in Fig. 6. One hairpin resonator is embedded in the other larger one with a gap of 0.04 mm. Their line width is 0.04 mm and their bottom lengths are 2.50 mm and 2.26 mm, respectively. The variables l_1 and l_2 represent their arm lengths, and d is the separation between their bottoms, as shown in Fig. 6. This closely coupled structure matches the proportional topology, shown in Fig. 4. This kind of dual-mode resonators can be cascaded to form a filter with the proposed topology, as shown in Fig. 5. As discussed above, this dual-mode resonator must have an ω_m between its two resonant frequencies, which is suitable to design high-isolation dual-mode dual-band filters.

From (32), Ω_a, Ω_b and m should be carefully designed to obtain a suitable transformation frequency. The variables l_1 and l_2 primarily affect Ω_a and Ω_b, respectively, and the distance, d affects the coupling coefficient, m in (32).

It is difficult to use l_1, l_2 and d to calculate Ω_{dual} accurately. However, the variables, l_1, l_2 and d are enough to design a suitable ω_1, ω_2 and ω_m. Fig. 7 shows the variation of ω_1, ω_2 and ω_m with l_1, l_2 and d for this resonator. Fig. 7(a) shows that l_1 primarily affects ω_1; Fig. 7(b) shows that l_2 primarily affects ω_2 and ω_m; and Fig. 7(c) shows that d primarily affects ω_m. Fig. 7 also shows that regardless of variations in l_1, l_2 and d change, the ω_m remains between ω_1 and ω_2, which validates this technique.

Let us design a dual band filter with two passbands from 4.22 GHz to 4.28 GHz and from 4.69 GHz to 4.82GHz, respectively. From [11], $\gamma = 24$, $\omega_1 = 2\pi{\cdot}4.25{\cdot}10^9$ rad/s $= 2\pi\cdot 4.25$ Grad/s, $\omega_2 = 2\pi\cdot 4.75$ Grad/s, $\omega_m = 2\pi\cdot 4.43$ Grad/s. To make our derivation clearly, all the units of the angular momentum (ω) in the following paper are Grad/s. So

$$\Omega_{dual} = 24\cdot\frac{(\omega^2-(2\pi\cdot 4.25)^2)(\omega^2-(2\pi\cdot 4.75)^2)}{\omega^2(\omega^2-(2\pi\cdot 4.43)^2)} \tag{34}$$

From (33), one solution for these equations is

$$\begin{aligned}\Omega_a &= 339\cdot\frac{\omega^2-(2\pi\cdot 4.32)^2}{\omega^2} \\ \Omega_b &= 18\cdot\frac{\omega^2-(2\pi\cdot 4.66)^2}{\omega^2} \\ \lambda &= 0.85 \\ m &= 5.94\end{aligned} \tag{35}$$

By optimizing l_1, l_2 and d, we can get

$$l_1 = 4.90 \text{ mm}, \quad l_2 = 4.40 \text{ mm}, \quad d = 0.24 \text{ mm} \tag{36}$$

Four dual-mode coupled hairpin resonators, which contains eight single mode hairpin resonators, are cascaded in this example. Fig. 8(a) shows the original single-mode matrix, which contains four proportional sections. We compress these proportional sections one by one, as shown in Fig. 8, and finally obtain the dual-mode matrix, shown in 8(e), which is the Chebyshev coupling matrix with 20-dB in-band return loss.

From [11], the coupling coefficient, k, for dual-mode resonators can be extracted:

$$|k| = \frac{f_2^2f_4^2 - f_1^2f_3^2}{f_2^2f_4^2 + f_1^2f_3^2} \tag{37}$$

where f_1, f_2, f_3, f_4 are the peaks of two coupled dual-mode resonators' response from small to large.

The external quality factor, Q_e can be extracted:

$$\frac{1}{Q_e} = \frac{4}{\omega_1\tau_{S_{11}}(\omega_1)} + \frac{4}{\omega_2\tau_{S_{11}}(\omega_2)} \tag{38}$$

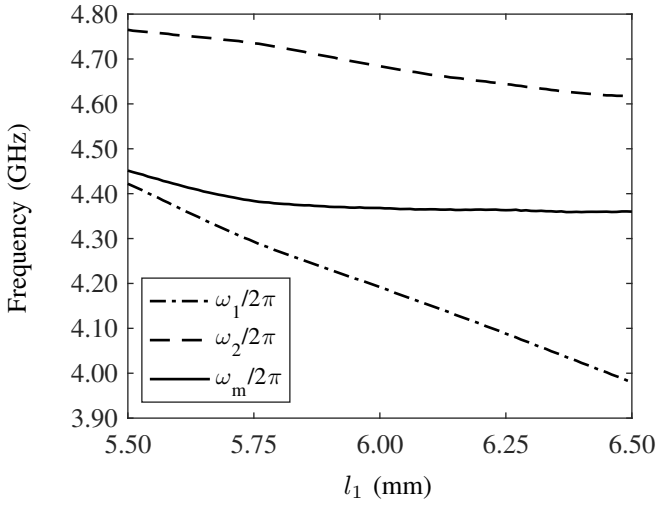

(a)

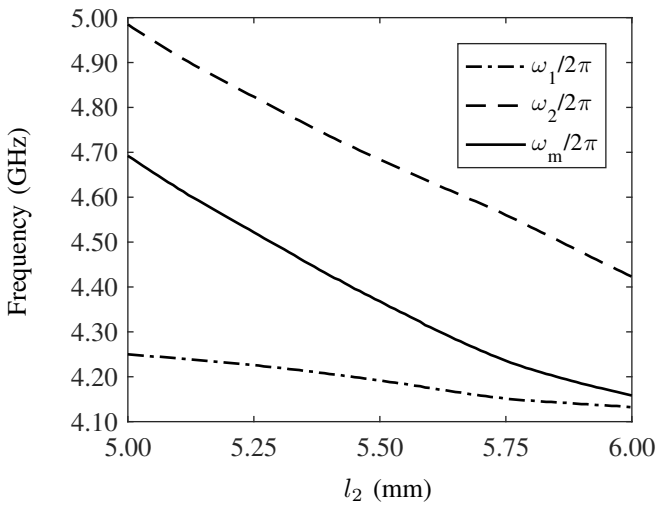

(b)

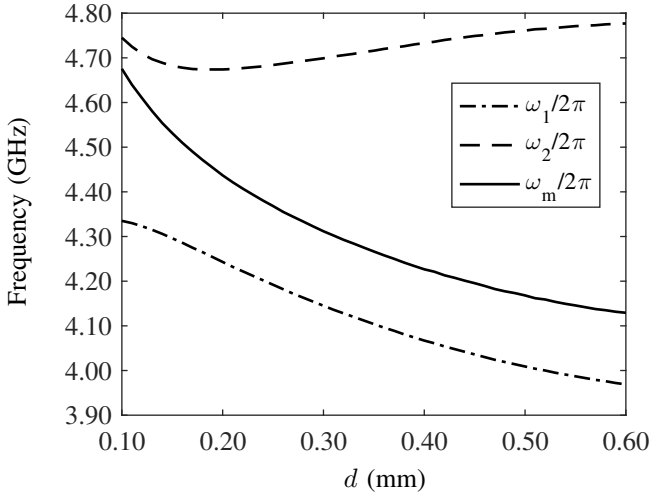

(c)

Fig. 7. Variation of ω_1, ω_2 and ω_m with l_1, l_2 and d. (a) l_1 variable, l_2=0.5 mm, d=0.25 mm; (b) l_2 variable, l_1=6 mm, d=0.25 mm; (c) d variable, l_1=6 mm, l_2=5.5 mm.

$$\begin{bmatrix}
-\mathrm{j} & 1.04 & 0.88 & 0 & 0 & 0 & 0 & 0 & 0 & 0 \\
1.04 & \Omega_a & 5.94 & 0.91 & 0.77 & 0 & 0 & 0 & 0 & 0 \\
0.88 & 5.94 & \Omega_b & 0.77 & 0.66 & 0 & 0 & 0 & 0 & 0 \\
0 & 0.91 & 0.77 & \Omega_a & 5.94 & 0.70 & 0.59 & 0 & 0 & 0 \\
0 & 0.77 & 0.66 & 5.94 & \Omega_b & 0.59 & 0.51 & 0 & 0 & 0 \\
0 & 0 & 0 & 0.70 & 0.59 & \Omega_a & 5.94 & 0.91 & 0.77 & 0 \\
0 & 0 & 0 & 0.59 & 0.51 & 5.94 & \Omega_b & 0.77 & 0.66 & 0 \\
0 & 0 & 0 & 0 & 0 & 0.91 & 0.77 & \Omega_a & 5.94 & 1.04 \\
0 & 0 & 0 & 0 & 0 & 0.77 & 0.66 & 5.94 & \Omega_b & 0.88 \\
0 & 0 & 0 & 0 & 0 & 0 & 0 & 1.04 & 0.88 & -\mathrm{j}
\end{bmatrix}$$

(a)

$$\begin{bmatrix}
-\mathrm{j} & 1.04 & 0 & 0 & 0 & 0 & 0 & 0 & 0 \\
1.04 & \Omega_{dual} & 0.91 & 0.77 & 0 & 0 & 0 & 0 & 0 \\
0 & 0.91 & \Omega_a & 5.94 & 0.70 & 0.59 & 0 & 0 & 0 \\
0 & 0.77 & 5.94 & \Omega_b & 0.59 & 0.51 & 0 & 0 & 0 \\
0 & 0 & 0.70 & 0.59 & \Omega_a & 5.94 & 0.91 & 0.77 & 0 \\
0 & 0 & 0.59 & 0.51 & 5.94 & \Omega_b & 0.77 & 0.66 & 0 \\
0 & 0 & 0 & 0 & 0.91 & 0.77 & \Omega_a & 5.94 & 1.04 \\
0 & 0 & 0 & 0 & 0.77 & 0.66 & 5.94 & \Omega_b & 0.88 \\
0 & 0 & 0 & 0 & 0 & 0 & 1.04 & 0.88 & -\mathrm{j}
\end{bmatrix}$$

(b)

$$\begin{bmatrix}
-\mathrm{j} & 1.04 & 0 & 0 & 0 & 0 & 0 & 0 \\
1.04 & \Omega_{dual} & 0.91 & 0 & 0 & 0 & 0 & 0 \\
0 & 0.91 & \Omega_{dual} & 0.70 & 0.59 & 0 & 0 & 0 \\
0 & 0 & 0.70 & \Omega_a & 5.94 & 0.91 & 0.77 & 0 \\
0 & 0 & 0.59 & 5.94 & \Omega_b & 0.77 & 0.66 & 0 \\
0 & 0 & 0 & 0.91 & 0.77 & \Omega_a & 5.94 & 1.04 \\
0 & 0 & 0 & 0.77 & 0.66 & 5.94 & \Omega_b & 0.88 \\
0 & 0 & 0 & 0 & 0 & 1.04 & 0.88 & -\mathrm{j}
\end{bmatrix}$$

(c)

$$\begin{bmatrix}
-\mathrm{j} & 1.04 & 0 & 0 & 0 & 0 & 0 \\
1.04 & \Omega_{dual} & 0.91 & 0 & 0 & 0 & 0 \\
0 & 0.91 & \Omega_{dual} & 0.70 & 0 & 0 & 0 \\
0 & 0 & 0.70 & \Omega_{dual} & 0.91 & 0.77 & 0 \\
0 & 0 & 0 & 0.91 & \Omega_a & 5.94 & 1.04 \\
0 & 0 & 0 & 0.77 & 5.94 & \Omega_b & 0.88 \\
0 & 0 & 0 & 0 & 1.04 & 0.88 & -\mathrm{j}
\end{bmatrix}$$

(d)

$$\begin{bmatrix}
-\mathrm{j} & 1.04 & 0 & 0 & 0 & 0 \\
1.04 & \Omega_{dual} & 0.91 & 0 & 0 & 0 \\
0 & 0.91 & \Omega_{dual} & 0.70 & 0 & 0 \\
0 & 0 & 0.70 & \Omega_{dual} & 0.91 & 0 \\
0 & 0 & 0 & 0.91 & \Omega_{dual} & 1.04 \\
0 & 0 & 0 & 0 & 1.04 & -\mathrm{j}
\end{bmatrix}$$

(e)

matrix compression

Fig. 8. Matrix compressed from a 10-dimension matrix to a 6-dimension matrix, where $\Omega_a = 339(\omega^2 - (2\pi \cdot 4.32)^2)/\omega^2$, $\Omega_b = 18(\omega^2 - (2\pi \cdot 4.66)^2)/\omega^2$, $\Omega_{dual} = 24(\omega^2 - (2\pi \cdot 4.25)^2)(\omega^2 - (2\pi \cdot 4.75)^2)/(\omega^2(\omega^2 - (2\pi \cdot 4.43)^2))$.

where $\tau_{S_{11}}(\omega_1)$ and $\tau_{S_{11}}(\omega_2)$ are the group delays for S_{11} at ω_1 and ω_2, respectively.

The layout of this filter is shown in Fig. 9(a). It is fabricated on a 0.51-mm thick MgO substrate with two-side YBCO HTS films. Fig. 9(b) shows a picture of this filter, and its simulated and measurement response is show in Fig. 9(c).

IV. Conclusion

This paper proposes coupling matrix compression technique, which can reduce the dimension of the coupling matrix.

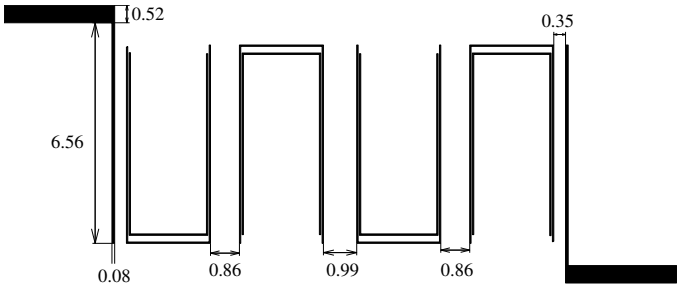

(a)

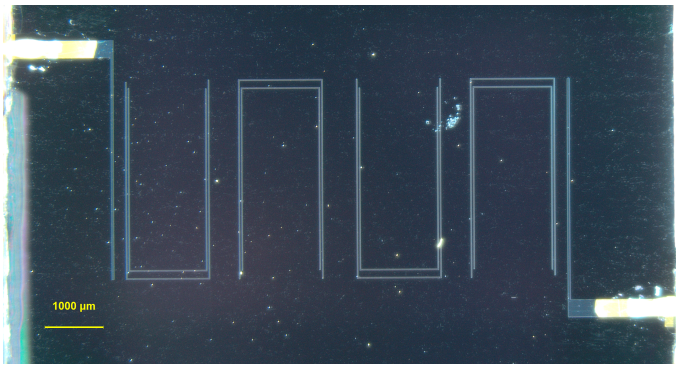

(b)

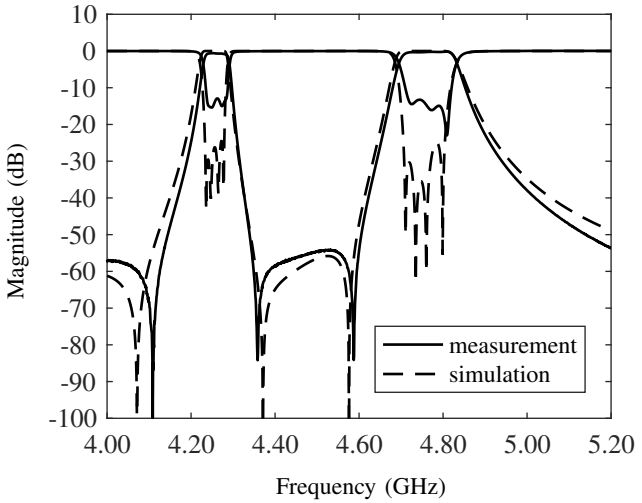

(c)

Fig. 9. (a) Layout of the designed dual-band filter (dimensions in mm). (b) Photograph of the filter. (c) Simulated and measured response.

A type of dual-mode resonators is proposed and analyzed, and the associated frequency transformation formula is derived. It is shown that the proposed dual-mode resonators can be used to design high-isolation dual-band filters. An embedded dual-mode hairpin resonator is studied. It is used for a dual-band filter. The measured and simulated results agree well with each other.

APPENDIX A
PROOF OF THE SCALING TRANSFORM

Consider the cofactor matrices $[C]$ and $[C']$ of $[A]$ and $[A']$, respectively.

From [20],

$$\begin{aligned} S_{21}(A') &= -2\mathrm{j}[A']^{-1}_{n+1,0} = -2\mathrm{j}\frac{[C']_{0,n+1}}{\det(A')} \\ &= -2\mathrm{j}\frac{\alpha^2[C]_{0,n+1}}{\alpha^2\det(A)} = -2\mathrm{j}\frac{[C]_{0,n+1}}{\det(A)} \\ &= -2\mathrm{j}[A]^{-1}_{n+1,0} = S_{21}(A) \end{aligned} \tag{39}$$

Similarly, we can prove that $S_{11}(A') = S_{11}(A)$, $S_{12}(A') = S_{12}(A)$ and $S_{21}(A') = S_{21}(A)$.

So $[A]$ and $[A']$ are equivalent.

APPENDIX B
PROOF ω_m IS BETWEEN ω_1 AND ω_2 WHEN $\gamma_a, \gamma_b > 0$

From (32), ω_1 and ω_2 are the roots of $\Omega_a\Omega_b - m^2 = 0$, and ω_m is the root of $\lambda^2\Omega_a + \Omega_b - 2\lambda m = 0$. Thus,

$$\begin{aligned} &\Omega_a(\omega_1)\Omega_b(\omega_1) = \Omega_a(\omega_2)\Omega_b(\omega_2) = m^2 \\ &\lambda^2\Omega_a(\omega_m) + \Omega_b(\omega_m) = 2\lambda m \end{aligned} \tag{40}$$

Because $\gamma_a, \gamma_b > 0$, $\Omega_a(\omega)$ and $\Omega_b(\omega)$ are both increasing functions. We assume that $\omega_1 < \omega_2$, then,

$$\Omega_a(\omega_1) < 0 < \Omega_a(\omega_2), \quad \Omega_b(\omega_1) < 0 < \Omega_b(\omega_2) \tag{41}$$

We define a function:

$$F(\omega) = \lambda^2\Omega_a(\omega) + \Omega_b(\omega) \tag{42}$$

It is obvious that $F(\omega)$ is an increasing function. Additionally, from (40),

$$F(\omega_m) = \lambda^2\Omega_a(\omega_m) + \Omega_b(\omega_m) = 2\lambda m \tag{43}$$

Then

$$\begin{aligned} F(\omega_2) &= \lambda^2\Omega_a(\omega_2) + \Omega_b(\omega_2) \\ &\geq 2\sqrt{\lambda^2\Omega_a(\omega_2)\Omega_b(\omega_2)} \\ &= 2\sqrt{\lambda^2 m^2} \\ &= |F(\omega_m)| \\ &\geq F(\omega_m) \end{aligned} \tag{44}$$

and

$$\begin{aligned} -F(\omega_1) &= \lambda^2|\Omega_a(\omega_1)| + |\Omega_b(\omega_1)| \\ &\geq 2\sqrt{\lambda^2\Omega_a(\omega_1)\Omega_b(\omega_1)} \\ &= 2\sqrt{\lambda^2 m^2} \\ &= |F(\omega_m)| \\ &\geq -F(\omega_m) \end{aligned} \tag{45}$$

Thus,

$$F(\omega_1) \leq F(\omega_m) \leq F(\omega_2) \tag{46}$$

Because $F(\omega)$ is an increasing function, we have

$$\omega_1 \leq \omega_m \leq \omega_2 \tag{47}$$

REFERENCES

[1] R. J. Cameron, "Advanced coupling matrix synthesis techniques for microwave filters," *IEEE Trans. Microw. Theory Techn.*, vol. 51, no. 1, pp. 1–10, 2003.

[2] R. J. Cameron, A. R. Harish, and C. J. Radcliffe, "Synthesis of advanced microwave filters without diagonal cross-couplings," *IEEE Trans. Microw. Theory Techn.*, vol. 50, no. 12, pp. 2862–2872, Dec. 2002.

[3] R. J. Cameron, "General coupling matrix synthesis methods for chebyshev filtering functions," *IEEE Trans. Microw. Theory Techn.*, vol. 47, no. 4, pp. 433–442, Apr. 1999.

[4] V. Miraftab and M. Yu, "Advanced coupling matrix and admittance function synthesis techniques for dissipative microwave filters," *IEEE Trans. Microw. Theory Techn.*, vol. 57, no. 10, pp. 2429–2438, Oct. 2009.

[5] R. J. Cameron, R. Mansour, and C. M. Kudsia, *Microwave filters for communication systems: fundamentals, design and applications*. Wiley-Interscience, 2007.

[6] V. Miraftab and M. Yu, "Generalized lossy microwave filter coupling matrix synthesis and design using mixed technologies," *IEEE Trans. Microw. Theory Techn.*, vol. 56, no. 12, pp. 3016–3027, Dec. 2008.

[7] S. Amari, "Synthesis of cross-coupled resonator filters using an analytical gradient-based optimization technique," *IEEE Trans. Microw. Theory Techn.*, vol. 48, no. 9, pp. 1559–1564, Sept. 2000.

[8] Y. T. Kuo, J. C. Lu, C. K. Liao, and C. Y. Chang, "New multiband coupling matrix synthesis technique and its microstrip implementation," *IEEE Trans. Microw. Theory Techn.*, vol. 58, no. 7, pp. 1840–1850, Jul. 2010.

[9] M. Mokhtaari, J. Bornemann, K. Rambabu, and S. Amari, "Coupling-matrix design of dual and triple passband filters," *IEEE Trans. Microw. Theory Techn.*, vol. 54, no. 11, pp. 3940–3946, Nov. 2006.

[10] R. J. Cameron, M. Yu, and Y. Wang, "Direct-coupled microwave filters with single and dual stopbands," *IEEE Trans. Microw. Theory Techn.*, vol. 53, no. 11, pp. 3288–3297, Nov. 2005.

[11] P. Ma, B. Wei, J. Hong, B. Cao, X. Guo, and L. Jiang, "Design of dual-mode dual-band superconducting filters," *IEEE Trans. Appl. Supercond.*, vol. 27, no. 7, pp. 1–9, Oct. 2017.

[12] J.-S. Hong, *Microstrip Filters for RF/Microwave Applications, 2nd Edition*. John Wiley & Sons, 2011.

[13] G. Macchiarella and S. Tamiazzo, "Design techniques for dual-passband filters," *IEEE Trans. Microw. Theory Techn.*, vol. 53, no. 11, pp. 3265–3271, Nov. 2005.

[14] A. S. Liu, T. Y. Huang, and R. B. Wu, "A dual wideband filter design using frequency mapping and stepped-impedance resonators," *IEEE Trans. Microw. Theory Techn.*, vol. 56, no. 12, pp. 2921–2929, Dec. 2008.

[15] Y. Heng and *et al.*, "Dual-band superconducting bandpass filter with embedded resonator structure," *Electron. Lett.*, vol. 49, no. 17, pp. 1096–1097, Aug. 2013.

[16] X. Y. Zhang and Q. Xue, "Harmonic-suppressed bandpass filter based on discriminating coupling," *IEEE Microw. Compon. Lett.*, vol. 19, no. 11, pp. 695–697, Nov. 2009.

[17] X. Y. Zhang, Q. Xue, C. H. Chan, and B. J. Hu, "Low-loss frequency-agile bandpass filters with controllable bandwidth and suppressed second harmonic," *IEEE Trans. Microw. Theory Techn.*, vol. 58, no. 6, pp. 1557–1564, Jun. 2010.

[18] M. A. Sanchez-Soriano, E. Bronchalo, and G. Torregrosa-Penalva, "Parallel-coupled line filter design from an energetic coupling approach," *IET Microw. Antenna. Propag.*, vol. 5, no. 5, pp. 568–575, Apr. 2011.

[19] M. A. Sanchez-Soriano, G. Torregrosa-Penalva, and E. Bronchalo, "Multispurious suppression in parallel-coupled line filters by means of coupling control," *IET Microw. Antenna. Propag.*, vol. 6, no. 11, pp. 1269–1276, Aug. 2012.

[20] D. Lay, S. Lay, and J. McDonald, *Linear Algebra and Its Applications, 5th Edition*. Pearson, 2015.

Pengyu Ma (S'16) was born in Henan, China, in 1993. He received the B.Sc. degree in applied physics from Tsinghua University, Beijing, China, in 2015. He is currently working toward Ph.D. degree in the Department of Physics, Tsinghua University, Beijing, China.

He is a reviewer for IEEE Transactions on Microwave Theory and Techniques. His current research interests include high-temperature superconducting materials and their application, RF and microwave circuits, theory of coupling matrix.

Bin Wei (M'12) was born in Zhejiang, China, in 1974. He received the B.Sc. and Ph.D. degrees in physics from Tsinghua University, Beijing, China, in 1996 and 2003, respectively. Since 2008, he has been an Associate Professor with the Department of Physics, Tsinghua University.

His current research interests include high-temperature superconducting microwave filters, HTS filter subsystems and their applications in wireless communications systems.

Jiasheng Hong (M'94-SM'05-F'12) received the D.Phil. degree in engineering science from the University of Oxford, Oxford, U.K., in 1994. His doctoral dissertation concerned EM theory and applications. In 1994, he joined the University of Birmingham, Birmingham, U.K., where he was involved with microwave applications of high-temperature superconductors, EM modeling, and circuit optimization. In 2001, he joined the Department of Electrical, Electronic and Computer Engineering, Heriot-Watt University, Edinburgh, U.K., and is currently a Professor leading a team for research into advanced RF/microwave device technologies. He has authored and coauthored over 200 journal and conference papers, and two books, Microstrip Filters for RF/Microwave Applications (Wiley, 1st ed., 2001, 2nd ed., 2011) and RF and Microwave Coupled-Line Circuits (Artech House, 2nd ed., 2007). His current interests involve RF/microwave devices, such as antennas and filters, for wireless communications and radar systems, as well as novel material and device technologies including multilayer circuit technologies using package materials such as liquid crystal polymer, RF MEMS, ferroelectric and high-temperature superconducting devices.

Xubo Guo (M'12) was born in Shanxi, China, in 1981. He received the B.Sc., M.Sc., and Ph.D. degrees in physics from Tsinghua University, Beijing, China, in 2001, 2004, and 2008, respectively. His doctoral research concerned high-power HTS filters.

From July 2008 to June 2010, he was a Postdoctoral Researcher with the Department of Electronic Engineering, Tsinghua University. Since July 2010, he has been an Engineer with the Department of Physics, Tsinghua University. He has authored and co-authored over 50 technical papers. His current research interests include HTS filters from VHF to Ka-band, as well as development and applications of HTS filter subsystems for mobile communications base stations and wireless receivers.

Bisong Cao was born in Jiangsu, China, in 1946. He received the B.Sc. and M.Sc. degrees in engineering physics from Tsinghua University, Beijing, China, in 1970 and 1981, respectively, and the Ph.D. degree in materials science from Tokyo University, Tokyo, Japan, in 1989.

He has been with the Department of Physics, Tsinghua University, since 1981, where he is currently a Professor. His current research interests include HTS physics and HTS microwave devices and their applications. He has published more than 100 papers in journals and international conference proceedings.

Prof. Cao is a Committee Member of the Superconductor Electronics Branch, Chinese Society for Electronics, and of the Low Temperature Physics Branch, Chinese Society for Physics.

Linan Jiang was born in Beijing, China, in 1986. He received the B.Sc. degree in applied physics from Beijing University of Technology, Beijing, China, in 2009.

Since 2009, he has been an Assistant Engineer with the Department of Physics, Tsinghua University, Beijing. His current research interests include high-temperature superconducting (HTS) microwave filters fabrication and HTS filter subsystems design and integration.